Thermionic emission and Gaussian transport of holes in a GaAs/$Al_xGa_{1-x}As$ multiple-quantum-well structure

H. Schneider and K. v. Klitzing
Max-Planck-Institut für Festkörperforschung, Heisenbergstrasse 1, D-7000 Stuttgart 80, Federal Republic of Germany
(Received 24 March 1988)

We present and test a modified thermionic emission model for time-resolved charge-carrier transport perpendicular to the layers of multiple quantum-well structures in an electric field. The predictions of the model on the nature (Gaussian transport) and the dynamics (transport times, field dependence of the mobility) of carrier transport agree favorably with our experiments performed for the case of holes and allow an accurate determination of the band offset.

I. INTRODUCTION

The study of carrier transport across semiconductor heterostructures is a field of growing interest for both basic research and potential applications. For thin barriers transport properties are dominated by tunneling processes. In the double barrier case one observes negative differential resistance due to resonant tunneling.[1] A similar effect occurs in multiple-quantum-well (MQW) structures when the electric field is such that different electronic subbands of neighboring wells have more or less the same energy.[2–4] For small electric fields and narrow barriers and wells the broadening of the subbands due to the quantum-mechanical coupling between the wells enables carrier transport within one subband (Bloch, miniband conduction).[5,6]

For thicker barriers tunneling processes are only dominant for very high electric fields when the barriers are triangular (Fowler-Nordheim regime). At moderate electric fields carriers must be transferred to higher-energy states (e.g., thermally activated) before crossing the barrier. Then Fowler-Nordheim tunneling only leads to a lowering of the effective barrier height.

In the conventional thermionic emission experiment one measures the temperature dependence of the (dc) current from a highly conducting region across a barrier. This method has been applied to Schottky[7] and semiconductor heterojunction[8] barriers.

In the present work we study the *dynamics* of thermionic emission in a MQW structure and relate the response times to the design parameters of the sample. Thus a more detailed experimental and theoretical understanding of the thermionic emission process is achieved. Some preliminary results have been published elsewhere.[9]

In Sec. II we present our modified thermionic emission model. The predicted shapes of photocurrent transients and transport times are compared with our experimental data in Sec. III. We give our conclusions in Sec. IV and some details of our model in the Appendixes.

II. THE MODEL

In order to obtain the emission rates we first consider an individual quantum well of width w in a MQW of period d. At a given electric field F we assume that the barriers to the right and left of the well are of the effective heights E_r and $E_l = E_r + deF$, respectively. So a carrier of charge e and effective mass m^* must be higher in energy than one of the barriers in order to be able to leave the well.

Consequently, as the electronic transport properties are determined by the occupation of states close to the top of the barrier, the application of a three-dimensional density of states and the use of Boltzmann statistics are good approximations. Then the carrier density dn in the well in an incremental energy range dE over the conduction- (or beyond the valence-) band edge E_C (E_V) is given by

$$dn = \frac{4\pi(2m^*)^{3/2}}{h^3}(E - E_{C,V})^{1/2}\exp\left[-\frac{E - E_F}{k_B T}\right]dE \ . \tag{1}$$

The quasi-Fermi-level E_F is determined by the total carrier density n_c in the well, i.e., by the condition

$$n_c = \int_{E_{C,V}}^{\infty} dn \ . \tag{2}$$

The emission currents J_r, J_l (in the x direction) over the barriers to the right and left, respectively, are given by

$$J_{r,l} = \int_{E_{r,l}}^{\infty} e v_x dn \ . \tag{3}$$

As in standard thermionic emission theory[7] the integrations in Eqs. (2) and (3) are easily carried out in velocity space (assuming that $E - E_C$ is kinetic energy) with the final result

$$J_{r,l} = e n_c \left[\frac{k_B T}{2\pi m^*}\right]^{1/2} \exp\left[-\frac{E_{r,l}}{k_B T}\right] . \tag{4}$$

From the continuity equation we get $w\dot{n}_c = -(J_r + J_l)/e$, which we write in the form

$$w\dot{n}_c = -\left[\frac{1}{\tau_r} + \frac{1}{\tau_l}\right] w n_c \tag{5}$$

with

$$\frac{1}{\tau_{r,l}}=\frac{1}{w}\left[\frac{k_BT}{2\pi m^*}\right]^{1/2}\exp\left[-\frac{E_{r,l}}{k_BT}\right]. \tag{6}$$

So the carrier population wn_c of the well decays by thermionic emission to the right and left with the time constants τ_r and τ_l, respectively.

Next we generalize this result to the MQW case. For simplicity (a more general case is discussed in Appendix B) we assume that the emitted carriers from one well are captured in the two neighboring wells. If $q_k(t)$ denotes the number of carriers in the kth well ($k=1,..,N$), we get the rate equations

$$\begin{aligned}\dot{q}_1&=-\left[\frac{1}{\tau_r}+\frac{1}{\tau_l}\right]q_1+\frac{1}{\tau_l}q_2\ ,\\ \dot{q}_k&=\frac{1}{\tau_r}q_{k-1}-\left[\frac{1}{\tau_r}+\frac{1}{\tau_l}\right]q_k+\frac{1}{\tau_l}q_{k+1}\ ,\\ \dot{q}_N&=\frac{1}{\tau_r}q_{N-1}-\left[\frac{1}{\tau_r}+\frac{1}{\tau_l}\right]q_N\ .\end{aligned} \tag{7}$$

If the charge at time $t=0$ is generated by a short light pulse, the initial condition reads

$$q_k(0)=Q_0\frac{1-\exp(-\alpha d)}{1-\exp(-\alpha Nd)}\exp[-\alpha(k-1)d] \tag{8}$$

with the total photogenerated charge Q_0 and the absorption coefficient α.

For the situation that the current to the left can be neglected ($1/\tau_r \gg 1/\tau_l \approx 0$) we briefly mention that the solution of the rate equations reads (omitting the index of τ_r)

$$\begin{bmatrix}q_1(t)\\ \vdots\\ q_N(t)\end{bmatrix}=e^{-t/\tau}\begin{bmatrix}1 & 0 & \cdots & \ddots & 0\\ \frac{t}{\tau} & 1 & 0 & & 0\\ \vdots & & \ddots & & \vdots\\ & & & 1 & 0\\ \frac{\left[\frac{t}{\tau}\right]^{N-1}}{(N-1)!} & \cdots & & \frac{t}{\tau} & 1\end{bmatrix}\begin{bmatrix}q_1(0)\\ \vdots\\ q_N(0)\end{bmatrix}. \tag{9}$$

From Eq. (A10) of Appendix A it is then easy to write down an explicit solution for the total current $j(t)$.

In the following we show that for large N there is a close correspondence between Eq. (7) and Gaussian transport. For this purpose we introduce the carrier density $n(x,t)$. If we put $x_k=kd$, $q_k(t)$ should be replaced by $den(x_k,t)$. Hence, neglecting higher-order terms, we get from Eq. (7) by Taylor expansion

$$\frac{\partial n}{\partial t}=-v\frac{\partial n}{\partial x}+\tfrac{1}{2}D\frac{\partial^2 n}{\partial x^2}\ , \tag{10}$$

where we have defined the drift velocity

$$v=d\left[\frac{1}{\tau_r}-\frac{1}{\tau_l}\right] \tag{11}$$

and the diffusion constant

$$D=d^2\left[\frac{1}{\tau_r}+\frac{1}{\tau_l}\right]. \tag{12}$$

It is trivial to express Eq. (11) in terms of a field-dependent mobility μ (which remains finite for $F\to 0$). A well-known solution of (10) is the Gaussian propagator function

$$g(x,t)=\frac{1}{\sqrt{2\pi Dt}}\exp\left[-\frac{(x-vt)^2}{2Dt}\right]. \tag{13}$$

Note that, from Eq. (13), Dt naturally appears as the variance of g:

$$Dt=\langle x^2-\langle x\rangle^2\rangle\,|_g\ . \tag{14}$$

As g has the property $g(x,0)=\delta(x)$ with the Dirac distribution $\delta(x)$, the solution of (10) with an appropriate initial condition $n(x,0)=n_0(x)$ is given by

$$n(x,t)=\int g(x-y)n_0(y)dy\ . \tag{15}$$

We take into account the absorbing boundaries at the edges $x=0$ and $x=L$ of the sample of thickness $L=Nd$ approximately by restricting the integration in Eq. (15) to the interval $[0,L]$.

As shown in Appendix A, the total current density j is then given by

$$j(t)=\frac{ev}{L}\int_0^L\int_0^L g(x-y)n_0(y)dx\,dy\ , \tag{16}$$

and the integration over the x variable can be done analytically in terms of the Gaussian error function. Finally we mention that, both in the discrete and in the continuous case, it is trivial to include an additional recombination process with time constant $\tau_{\rm rec}$ which just gives an extra factor $\exp(-t/\tau_{\rm rec})$ in the occurring carrier populations and current densities.

III. EXPERIMENTAL RESULTS AND DISCUSSION

For an experimental test of our model we chose a 100-period GaAs/Al_xGa_xAs MQW structure. The undoped MQW is sandwiched between window layers of 300-nm n^+-type $Al_{0.5}Ga_{0.5}As$ on the substrate side and 800-nm p^+-type $Al_{0.5}Ga_{0.5}As$ on the top side. The structure is grown by molecular-beam epitaxy on a (100)-oriented n^+-type GaAs substrate and processed into mesas of 0.27 mm^2 active area with CrAu Ohmic contacts. The n^+-type $Al_{0.5}Ga_{0.5}As$ layer serving as an etch stop, the substrate beyond the active area of some of the samples is removed.

The barrier and well widths $b=13.5$ nm and $w=12.1$ nm, respectively, are determined by x-ray diffraction (with a slight difference to the designated values of Ref. 9). The *actual* Al content x of the barriers of the MQW is determined by theoretical fits to the x-ray diffraction

curves[10] with the result $x = (33.0 \pm 0.4\,\%)$.

For our measurements we use a nitrogen-pumped dye laser (500 ps pulse length, 5 Hz repetition rate) to excite the MQW structure and a TEK 7912AD transient recorder to detect the time-resolved photocurrent which is averaged over several hundred shots and corrected for the dark signal.

In order to minimize space-charge effect we apply pulsed bias and measure the photocurrent transients at low excitation density ($\approx 10^{13}$ cm^{-3}). In our measurements there is a large difference between the shape of the transients obtained with pulsed and dc bias (Fig. 1) which we understand in the following way. One sort of carriers (electrons) is captured very effectively by some traps for a time much longer than the repetition time of the laser. In the dc-bias case this causes a gradual development of space charges in the MQW region. As can be calculated from the Poisson equation, these space charges give rise to a band bending which influences the signal. For pulsed bias, however, space charges are reduced: During the switch-off time of the voltage, the band bending lead to an injection of carriers (holes) at one contact and a subsequent neutralization of space charges by recombination. This interpretation is confirmed by the fact that the shape of the transient only depends on the *length* of the pause between the bias pulses and is independent of the *temporal position* with respect to the laser shots. We conclude from our experiments that the mentioned carrier injection occurs within a few μs. Hence the transients should be due to the motion of one sort of carriers (holes), and we may actually take a one-carrier model to describe the data. We mention that these arguments hold for drifting electrons and trapped holes in the same way. The shape of the signal under different illumination conditions will demonstrate, however, that we are actually dealing with hole transport. Of course, at large excitation densities ($> 10^{15}$ cm^{-3}) the shape of the transients

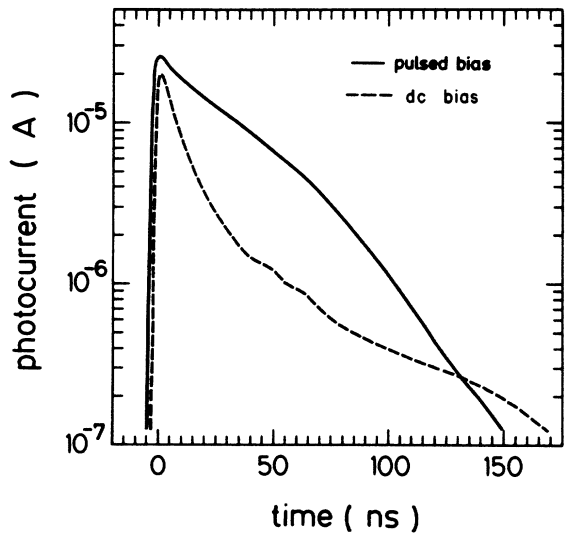

FIG. 1. Photocurrent transients at a temperature of 200 K, an electric field of 43.8 kV/cm and 780 nm front illumination using pulsed bias (solid line) and dc bias (dashed line).

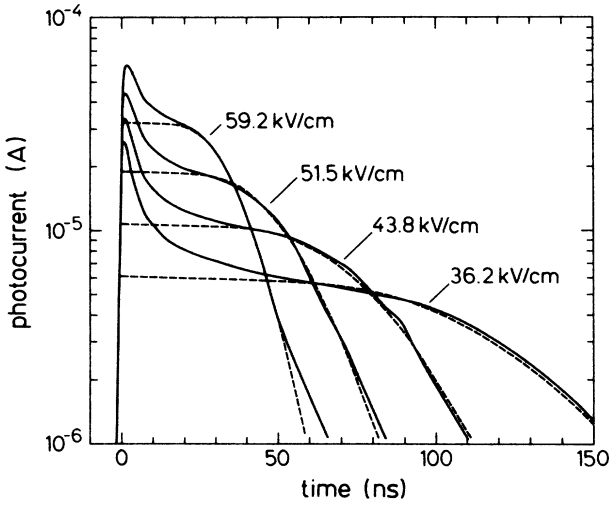

FIG. 2. Photocurrent transients (solid lines) and computer simulations (dashed lines) at 200 K, 540 nm backside illumination, and different electric fields, as indicated by the arrows.

becomes dependent on the density itself, and the difference between dc and pulsed bias is no longer important.

Some photocurrent transients (backside illumination by 540-nm laser pulses) at different electric fields are plotted in Fig. 2 (solid lines). The decay of the signal consists of an initial fast component and a subsequent slower one which becomes shorter for increasing electric field. We mention that at very high electric fields the duration of the signal is ultimately limited by the bandwidth (500 MHz) of the measurement system. As the fast component becomes more intensive with decreasing laser wavelength (and almost vanishes at near-band-gap excitation), we assign it to the motion of carriers generated in the contact and/or barrier regions.

The field-dependent slower component is well explained by our rate equation approach. We also plotted computer simulations (dashed lines in Fig. 2) to illustrate this. As the penetration depth at 540 nm is much smaller than the MQW thickness, the physical picture is the following: The plateau region of the transient comes from the motion of a sheet of photogenerated holes moving with an effective drift velocity v. At the same time, the sheet becomes spatially broadened due to the statistical nature of the thermionic emission process which can be cast into an effective diffusion constant D. Therefore, when the carriers are reaching the contact, the current vanishes gradually, not abruptly.

We mention that for frontside illumination (540-nm wavelength) the current transients are much shorter than for the former case and show a nearly exponential time dependence. This behavior is explained if we assume hole transport (i.e., the carriers must be generated near the contact they have to reach). As there is some temporal overlap with the initial fast component of the photocurrent transients which complicates the interpretation we will not present the data here.

Although, as will be shown later, the experimental drift velocities are in good agreement with the model, the

diffusion constant is too large by a factor of about 7. Note in this context that for $\tau_r \ll \tau_l$ the quantity D/v does not contain any time constants. One possibility to change the value of D/v is to assume that there is a finite probability that an emitted carrier is *not* captured in the neighboring wells. Such a model is given in Appendix B. Alternatively one could look for additional diffusion processes or relate the discrepancy to a slightly inhomogeneous electric field.

The large dependence of the photocurrent dynamics on the temperature is shown in Fig. 3 for an exciting wavelength of 780 nm (frontside illumination). Note that for the case of Fig. 3 the motion of the holes is opposite to the direction of the illumination. We estimate an absorption coefficient α of about 7000 cm^{-1} from computer simulations using our rate equation model. This value is in good agreement with ellipsometric data.[11]

We obtain an effective response time τ_{eff} by plotting the transient in a doubly logarithmic scale where the slope of the curve is minus one at the time τ_{eff} by definition. We mention that this procedure is exact for exponentials and coincides well with our computer simulations. For this purpose we use data obtained with 780-nm radiation in order to eliminate the influence of the initial fast component.

The result is given in Fig. 4. We point out that the temperature dependence of the response time τ_{eff} actually shows a thermally activated behavior. From a least-squares fit we obtain activation energies between 157 meV (at 20.8 kV/cm) and 135 meV (at 59.2 kV/cm). The electric field is obtained by dividing the sum of the built-in (about 1.4 V) and the applied voltage by the width L of the intrinsic region ($L = 2.6\ \mu m$).

We use an estimated drift length of $L/2$ and the drift velocity from Eqs. (6) and (11) to define a theoretical time constant $\tau = L/2v$ which can be compared with τ_{eff}. Note that this time constant τ only depends very weakly on the

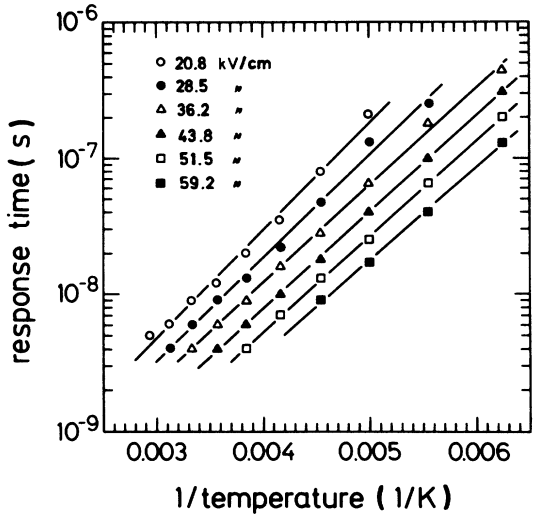

FIG. 4. Temperature dependence of the response time τ_{eff} (see text) at 780 nm front illumination and different electric fields, as indicated in the inset.

effective mass m^*. Weighting the heavy-hole (hh) and light-hole (lh) emission currents with the densities of states[7] we get

$$m^* = \left[\frac{m_l^{3/2} + m_h^{3/2}}{m_l + m_h} \right]^2 . \tag{17}$$

For our calculation we take $m_l = 0.094$ and $m_h = 0.34$ for the lh and hh masses (in units of free-electron masses), respectively.[12]

Inserting the activation energies obtained from the temperature dependence for the effective barrier height E, we find a good agreement between theory and experi-

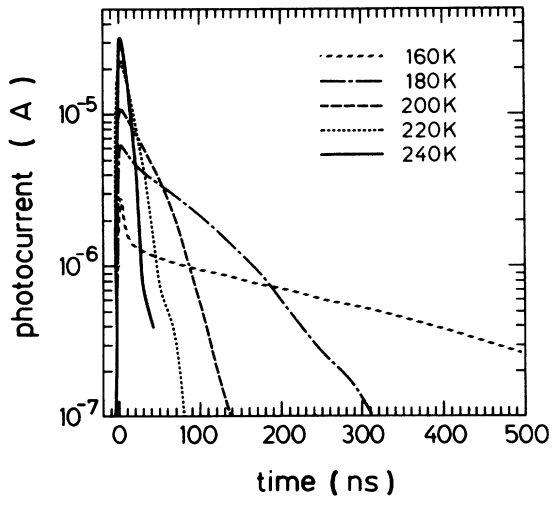

FIG. 3. Photocurrent transients at 43.8 kV/cm, 780 nm front illumination, and different temperatures, as indicated in the inset.

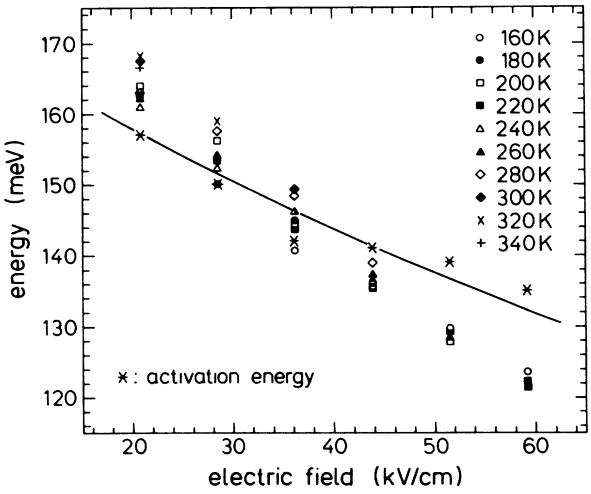

FIG. 5. Effective barrier potential energy calculated from the measured response time using Eq. (18) at different temperatures (indicated in the inset) and measured activation energy (open circles) vs electric field. The symbols correspond to different temperatures given in the inset. The solid line is a theoretical estimation (see text).

ment. Thus we can use our model to obtain the barrier height E directly from the experimental response time. To illustrate this we insert Eqs. (6) and (11) into the expression for τ and solve for E:

$$E = k_B T \ln \left\{ \frac{2d\tau}{Lw} \left[\frac{k_B T}{2\pi m^*} \right]^{1/2} \left[1 - \exp\left[-\frac{deF}{k_B T} \right] \right] \right\} . \tag{18}$$

Now we use this equation to calculate the effective barrier height from the experimental time constant τ_{eff}. The result is plotted in Fig. 5, together with the measured activation energies. From these data we conclude that, once the activation energy is known, our model predicts the correct value of the transport time within a factor of about 2. [This corresponds to a difference of $k_B T \ln 2$ between the energy from Eq. (18) and the measured activation energy.]

It is interesting to compare these energies with the quantum-mechanically expected effective barrier heights. We mention the two important effects: One is the field dependence of the lowest hole subbands with respect to the valence-band edge, the other is the lowering of the effective barrier height due to Fowler-Nordheim tunneling. For the carrier confinement we take the low-field limit[13] which is a better approximation for the range of electric fields applied in our measurements than an $F^{2/3}$ law. The Fowler-Nordheim reduction of the barrier height $E(F)$ (in the WKB approximation) is proportional to $F^{2/3}$. From this we obtain

$$E(F) = E(0) - \frac{eFw}{2} + C_{\text{pert}} \frac{m^* e^2 F^2 w^4}{\hbar^2} - C_{\text{FN}} \left[\frac{\hbar^2 e^2 F^2}{m^*} \right]^{1/3} . \tag{19}$$

The prefactors read $C_{\text{pert}} = (15/\pi^2 - 1)/(24\pi^2)$ (Ref. 13) and $C_{\text{FN}} = (\frac{9}{32})^{1/3}$ (WKB exponent set to -1) (Ref. 7), respectively. As $E(F)$ depends only weakly on m^* we take again the value from Eq. (17). (Alternatively we would have to reformulate our thermionic emission model for superposed lh and hh emission currents with slightly different activation energies). From the choice $E(0) = 177$ meV we get the solid curve plotted in Fig. 5.

The valence-band offset is estimated from a $\frac{57}{43}$ rule[12] for the conduction- and/or valence-band discontinuities to the value of 177 meV. This magnitude should differ from $E(0)$ by the confinement energy of the lowest subband for $F = 0$ which is about 6 meV for the hh case, so the agreement is very reasonable.

Concerning the data of Fig. 4 we point out that the activation energy is a *differential* property of the dynamic behavior, so most of the idealizations of our models concerning the *absolute* behavior of the transport time are eliminated.

IV. CONCLUSIONS

We presented a modified thermionic emission model for time-resolved carrier transport in MQW structures. From this model we made detailed predictions on the field and temperature dependence of the mobility in the thermionic emission case and on the shape of photocurrent transients (Gaussian transport).

These predictions coincide with our experiments observations on a 12.1-nm-GaAs/13.5-nm-$Al_{0.33}Ga_{0.67}As$ MQW structure embedded in a p^+-i-n^+-diode configuration. The data were used to determine the field-dependent height of the MQW barriers. We found the same behavior as expected from a quantum-mechanical reduction of the barrier height. We point out that our method can be used for a high-precision determination of band offsets as one only needs to study dynamical effects (response times) inside a depleted region. Such a situation requires fewer assumptions than in the conventional thermionic emission measurement where at least at one side of the barrier the carrier concentration is high and a dc current (stationary equilibrium) is measured.

ACKNOWLEDGMENTS

The authors are grateful to Dr. K. Ploog and Dr. S. Tarucha for providing the samples and for valuable discussions, to Dr. L. Tapfer for the high-precision x-ray characterization of our sample, and to Dr. W. Rühle for critical reading of the manuscript. Part of this work was sponsored by the Bundesministerium für Forschung und Technologie and the Stiftung Volkswagenwerk.

APPENDIX A

In the following we will determine the total current density $j(t)$ for a given carrier density $n(x,t)$ and apply the result to some cases of interest. The main point in our derivation will be that, in contrast to the usual textbook presentation, we calculate $j(t)$ *from the displacement current and not from the conduction current.* In this way we avoid an *a priori* relation between the conduction current and the electric field.

We start with the Poisson equation (SI units)

$$\frac{\partial F(x,t)}{\partial x} = \frac{e}{\epsilon} n(x,t) , \tag{A1}$$

the continuity equation for the conduction current j_c

$$\frac{\partial j_c(x,t)}{\partial x} = -e \frac{\partial n(x,t)}{\partial t} , \tag{A2}$$

and the boundary condition

$$\int_0^L F(x,t) dx = \Phi_0 \tag{A3}$$

which defines the total electrostatic potential Φ_0. From (A3) we get, the integration by parts,

$$\Phi_0 = LF(L,t) = \int_0^L x \frac{\partial F(x,t)}{\partial x} dx . \tag{A4}$$

Now we calculate $F(x,t)$ from (A1):

$$\epsilon F(x,t) = -e\int_x^L n(x,t)dx + \frac{e}{L}\int_0^L xn(x,t)dx + \frac{\epsilon}{L}\Phi_0 \ . \tag{A5}$$

From (A1) and (A2) it is clear that the total current density

$$j(t) = j_c(x,t) + \epsilon\frac{\partial F(x,t)}{\partial t} \tag{A6}$$

is not x dependent.

In order to determine $j(t)$ we assume that both $n(x,t)$ and $j_c(x,t)$ vanish at $x = L$. This means that for $x = L$ the displacement current $\epsilon\partial F/\partial t$ equals the total current, and we get from (A5) and (A6)

$$j(t) = \frac{e}{L}\int_0^L x\frac{\partial n(x,t)}{\partial t}dx \ . \tag{A7}$$

For vanishing n and j_c at $x = 0$ we have

$$j(t) = \frac{e}{L}\int_0^L (x-L)\frac{\partial n(x,t)}{\partial t}dx \ . \tag{A8}$$

If both (A7) and (A8) are valid, the charge

$$Q_0 = e\int_0^L n(x,t)dx \tag{A9}$$

is constant in time.

In the case of low excitation it is certainly a good approximation to neglect the effects of the boundary (e.g., by assuming a background density of immobile carriers of opposite charge). Then we can evaluate (A7) or (A8) for some special cases.

For the case of Eq. (7), (A7) leads to a summation,

$$j(t) = \frac{e}{N}\left[\frac{1}{\tau_r} - \frac{1}{\tau_l}\right]\sum_{k=1}^{N} q_k(t) \tag{A10}$$

modulo boundary terms, and for the case of Eq. (10), we get, after an integration by parts,

$$j(t) = \frac{v}{L}e\int_0^L n(x,t)dx \ . \tag{A11}$$

We note that (A10) and (A11) give the same physical drift velocity. From the explicit solution (9) of the discrete system, one can easily show via Eq. (14) that Eqs. (7) and (10) also lead to identical diffusion constants, at least for the case $1/\tau_l = 0$.

APPENDIX B

In generalization of Eq. (7), we will consider a system of rate equations describing carriers which, once emitted from a well, have finite probabilities p_r, p_l *not* to be absorbed in the right and left neighboring wells, respectively. Such a system reads

$$\frac{dq_k}{dt} = \frac{1-p_l}{p_l\tau_l}\sum_{m(\geq 1)} p_l^m q_{k-m} + \frac{1-p_r}{p_r\tau_r}\sum_{m(\geq 1)} p_r^m q_{k+m} - \left[\frac{1}{\tau_l} + \frac{1}{\tau_r}\right]q_k \ . \tag{B1}$$

Of course, (B1) approaches (7) if $p_l, p_r \to 0$. If p_l and p_r are small enough, we can proceed in the same way as earlier, so that Eqs. (10)–(12) are replaced by

$$\frac{\partial n}{\partial t}(x,t) = d\left[\frac{1-p_r}{p_r\tau_r}\sum_{m(\geq)1} mp_r^m - \frac{1-p_l}{p_l\tau_l}\sum_{m(\geq)1} mp_l^m\right]\frac{\partial n}{\partial x}(x,t) + \frac{d^2}{2}\left[\frac{1-p_r}{p_r\tau_r}\sum_{m(\geq 1)} m^2p_r^m + \frac{1-p_l}{p_l\tau_l}\sum_{m(\geq 1)} m^2p_l^m\right]\frac{\partial^2 n}{\partial x^2}(x,t) \ . \tag{B2}$$

Assuming the number of wells large enough, we neglect boundary effects. Working out the sums analytically, we arrive again at Eq. (7), but with the more general expressions

$$v = \frac{d}{\tau_r}\frac{1}{1-p_r} - \frac{d}{\tau_l}\frac{1}{1-p_l} \tag{B3}$$

and

$$D = \frac{d^2}{\tau_r}\frac{1+p_r}{(1-p_r)^2} + \frac{d^2}{\tau_l}\frac{1+p_l}{(1-p_l)^2} \tag{B4}$$

for the drift velocity and the diffusion constant, respectively. Note that D depends more sensitively on p_r, p_l than v.

[1] L. L. Chang, L. Esaki, and R. Tsu, Appl. Phys. Lett. **24**, 593 (1974).

[2] Y. Masumoto, S. Tarucha, and H. Okamoto, Phys. Rev. B **33**, 5961 (1985).

[3] M. J. Kelly, R. A. Davies, A. P. Long, N. R. Couch, P. H. Beton, and T. M. Kerr, Superlatt. Microstruct. **2**, 313 (1986).

[4] S. Tarucha, K. Ploog, and K. v. Klitzing, Phys. Rev. B **36**, 4558 (1987).

[5] J. F. Palmier, H. Le Person, C. Minot, A. Chomette, A. Regreny, and D. Calecki, Superlatt. Microstruct. **1**, 67 (1985).

[6] C. Minot, H. Le Person, F. Alexandre, and J. F. Palmier, Appl. Phys. Lett. **51**, 1626 (1987).

[7] S. M. Sze, *Physics of Semiconductor Devices*, 2nd ed. (Wiley, New York, 1981).

[8] P. M. Solomon, S. L. Wright, and C. Lanza, Superlatt. Microstruct. **2**, 521 (1986).

[9] H. Schneider, K. v. Klitzing, and K. Ploog, J. Phys. (Paris) Colloq. **48**, C5-431 (1987).

[10] L. Tapfer and K. Ploog, Phys. Rev. B **33**, 5565 (1986).

[11] D. E. Aspnes, S. M. Kelso, R. A. Logan, and R. Bhat, J. Appl. Phys. **60**, 754 (1986).

[12] R. C. Miller, D. A. Kleinmann, and A. C. Gossard, Phys. Rev. B **29**, 7085 (1984).

[13] G. Bastard, E. E. Mendex, L. L. Chang, and L. Esaki, Phys. Rev. B **28**, 3241 (1983).